

# Optical manipulation of bipolarons in a system with nonlinear electron-phonon coupling

K. Kovač,<sup>1</sup> D. Golež,<sup>1,2</sup> M. Mierzejewski,<sup>3</sup> and J. Bonča<sup>1,2</sup>

<sup>1</sup>*J. Stefan Institute, 1000 Ljubljana, Slovenia*

<sup>2</sup>*Faculty of Mathematics and Physics, University of Ljubljana, 1000 Ljubljana, Slovenia*

<sup>3</sup>*Department of Theoretical Physics, Faculty of Fundamental Problems of Technology, Wrocław University of Science and Technology, 50-370 Wrocław, Poland*

(Dated: May 17, 2023)

We investigate full quantum mechanical evolution of two electrons nonlinearly coupled to quantum phonons and simulate the dynamical response of the system subject to a short spatially uniform optical pulse that couples to dipole-active vibrational modes. Nonlinear electron-phonon coupling can either soften or stiffen the phonon frequency in the presence of electron density. In the former case, an external optical pulse tuned just below the phonon frequency generates attraction between electrons and leads to a long-lived bound state even after the optical pulse is switched off. It originates from a dynamical modification of the self-trapping potential that induces a metastable state. By increasing the pulse frequency, the attractive electron-electron interaction changes to repulsive. Two sequential optical pulses with different frequencies can switch between attractive and repulsive interaction. Pulse-induced binding or repulsion of electrons is shown to be efficient also for weakly dispersive optical phonons and in the presence of weak Coulomb repulsion.

PACS numbers:

Research in the field of driven quantum materials is at the forefront of modern solid-state physics. The development of new laser sources opened a new chapter in the field<sup>1</sup> where we can selectively excite collective degrees of freedom, like lattice, magnetic and electronic excitations, to generate new emergent states of matter<sup>2-4</sup>. Among the most prominent examples are optical manipulation of magnetic order<sup>5-8</sup>, light-induced non-equilibrium metal-insulator transitions<sup>9-13</sup>, and optically enhanced transient states displaying superconducting signatures<sup>2,14-23</sup>.

Modifying superconducting transition temperature by external stimulus was first shown using microwave radiation, now known as the Wyatt-Dayem effect<sup>24-26</sup>. More recently, it has been suggested that the selective excitation of a system could dramatically enhance the effect on the electronic system with nonlinear lattice couplings. A classic example includes a nonlinear coupling between optically excited infrared active mode inducing a Raman mode distortion<sup>12,27-29</sup> with modified electronic properties. The idea was applied to cuprate superconductors<sup>30</sup>, metal-insulator transition in manganites<sup>9,31</sup> and paraelectric-ferroelectric transition in SrTiO<sub>3</sub><sup>32,33</sup>. An even more interesting class of scenarios explores the role of quantum mechanical fluctuations on pairing from nonlinear phononics. In equilibrium, the nonlinear electron-phonon (EP) coupling leads to light polarons<sup>34</sup> and even more significantly to strongly bound light bipolarons<sup>35</sup>. Out of equilibrium, the squeezed electronic states due to nonlinear electron-lattice coupling can induce attraction between charge carriers inducing either superconducting<sup>36</sup> or insulator-metal transition<sup>37,38</sup>. The second class of ideas is based on the parametric resonance effect, where the interplay of driving and lattice non-linearities leads to enhanced electron-phonon interaction and pairing<sup>18</sup>. However, other studies point out the competition between pairing, heating or phonon-induced disorder and, depending on the approximation employed, one or another could prevail<sup>39,40</sup>. Therefore, obtaining exact results for a driven system to understand the competition and gauge

which approximations are appropriate for these highly excited correlated states would be highly valuable.

In this Letter, we provide an exact time evolution of a two-electron system coupled non-linearly to lattice distortions and driven by an external laser pulse, which homogeneously excites dipolar active lattice modes. We show that electronic binding can be dramatically enhanced or reduced depending on the pulse protocol. The electron binding (or repulsion) remains enhanced due to modified bipolaronic self-trapping leading to a long-lived (metastable) state even after the pulse has been switched off. We show that the binding takes place only for negative values of non-linear electron-lattice couplings (frequency softening), which is in contrast with previously applied approximation predicting a sign independent binding<sup>18,36,38,40</sup>. Finally, we show that the metastable state slowly decays if Einstein phonons acquire a finite bandwidth, still, the binding remains elevated in comparison to its value before the application of the pulse.

The model under the consideration is given by

$$H_0 = -t_{\text{el}} \sum_{j,s} (c_{j,s}^\dagger c_{j+1,s} + \text{H.c.}) + g_2 \sum_j \hat{n}_j (a_j^\dagger + a_j)^2 + \omega_0 \sum_j a_j^\dagger a_j + U \sum_j n_{i,\uparrow} n_{i,\downarrow}, \quad (1)$$

where  $c_{j,s}^\dagger$  and  $a_j^\dagger$  are electron and phonon creation operators at site  $j$  and spin  $s$ , respectively,  $\hat{n}_j = \sum_s c_{j,s}^\dagger c_{j,s}$  represents the electron density operator,  $t_{\text{el}}$  the nearest-neighbor electron hopping amplitude, and  $\omega_0$  denotes the Einstein phonon frequency. From here and on we set  $t_{\text{el}} = 1$ . The second term in Eq. (1) represents a quadratic EP coupling, and the last term the on-site Coulomb repulsion.

Since the studied Hamiltonian exists in infinitely dimensional Hilbert space one needs to single out a subspace that is relevant for the studied problem. Here, we focus on the dynamics of electrons thus the relevant subspace contains states where multiple phononic excitations may exist in the neigh-

borhood of electrons. More distant phononic excitations are discarded since they do not influence the distribution of electrons. In order to construct such subspace we have used a numerical method described in detail in Refs.<sup>41–46</sup> as well as in the Supplemental information (SM).<sup>47</sup> The method contains a single parameter  $N_h$  that determines the maximal distance between electrons as well as the maximal number of phonon excitations.

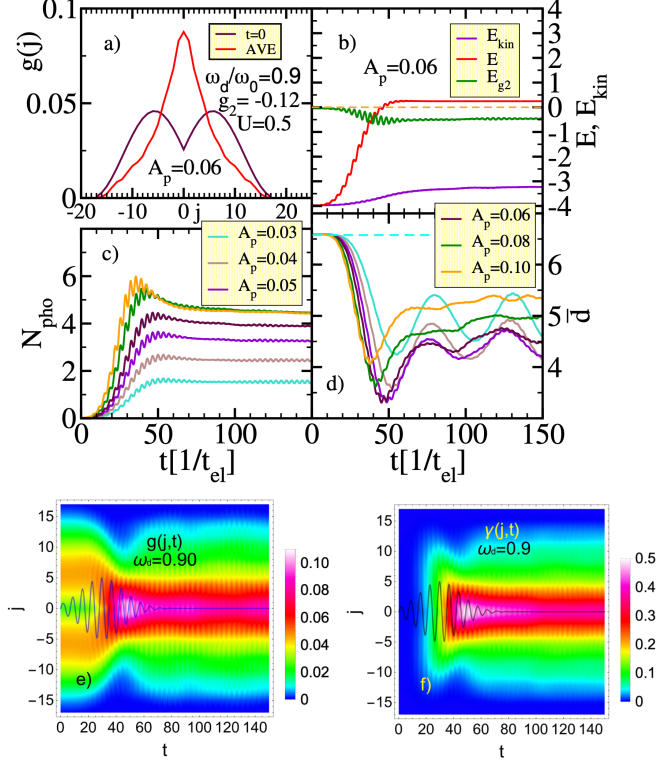


Figure 1: Different expectation values: a) the density–density correlation function in the ground state  $g(j, t = 0)$  and time-averaged  $\bar{g}(j)$  in the time interval  $[45-150]$  after the pulse  $V(t)$  with amplitude  $A_p = 0.06$ ,  $\sigma = 15$ ,  $t_0 = 30$ , and frequency  $\omega_d/\omega_0 = 0.9$ ; b) the total energy  $E(t) = \langle H \rangle_t$ , the kinetic energy  $E_{\text{kin}}(t) = \langle H_{\text{kin}} \rangle_t$  and EP coupling energy  $E_{g_2}(t) = \langle H_{g_2} \rangle_t$  where  $H_{\text{kin}}$  and  $H_{g_2}$  represent the first and the second term in Eq. (1), respectively; c) the total number of phonon excitations  $N_{\text{pho}} = \langle \sum_j a_j^\dagger a_j \rangle_t$  at different pulse amplitudes  $A_p$ ; d) the average particle distance  $\bar{d}$ ; e) the density–density correlation function  $g(j, t)$ ; f) the number of phonons as a function of the inter–electron distance  $\gamma(j, t)$ ; in e) and f) we used  $A_p = 0.06$  and the shape of the pulse  $V(t)$  is shown, its vertical scale is in arbitrary units. In all figures, the driving frequency is  $\omega_d/\omega_0 = 0.9$  and the electron-phonon coupling is  $g_2 = -0.12$ .

We excite the system by driving an infrared active mode  $H(t) = H_0 + V(t) \sum_j (a_j^\dagger + a_j)$  with a classical uniform AC field  $V(t) = A_p \sin(\omega_d t) \exp[-(t - t_0)^2/2\sigma^2]$  that couples uniformly to all lattice displacements and time-propagate the full problem using the standard Lanczos procedure<sup>48</sup>. Our first observable is the time evolution of the density–density

operator

$$\hat{g}(j) = \sum_i \hat{n}_{i,\uparrow} \hat{n}_{i+j,\downarrow}; \quad g(j, t) = \langle \hat{g}(j) \rangle_t, \quad (2)$$

where we use the following notation  $\langle \hat{A} \rangle_t = \langle \psi(t) | \hat{A} | \psi(t) \rangle$ . In the case of two electrons with the opposite spins, the operator  $\hat{g}(j)$  is a projector which singles out states for which the distance between both electrons equals  $j$  and the average distance between electrons can be obtained as  $\bar{d}(t) = \sum_j |j| g(j, t)$ .

In Fig. 1 a) we present  $g(j, t = 0)$  in the initial ground state of the system using a small Coulomb repulsion  $U = 0.5$  that overcomes a weak phonon-mediated attraction. Functional dependence of  $g(j, t = 0)$  is consistent with two electrons at an average distance  $\bar{d}(t = 0) \sim 6.5$  as also seen from Fig. 1 d). Switching on the pulse  $V(t)$  with a characteristic frequency  $\omega_d/\omega_0 = 0.9$  and different amplitudes  $A_p$  causes the increase of the total and kinetic energies,  $E$  and  $E_{\text{kin}}$ , respectively, and a slight decrease of EP coupling energy  $E_{g_2}$ , see Fig. 1 b). For definitions see the caption of Fig. 1. The increase of  $E$  is predominantly due to the increase of the total number of phonon quanta  $N_{\text{pho}}$ , shown in Fig. 1 c). The most notable effect of the pulse is a substantial decrease of the average distance  $\bar{d}$  between electrons, seen in Fig. 1 d). While the increase of  $N_{\text{pho}}$  with increasing  $A_p$  up to  $A_p = 0.08$  is monotonous, the decrease of  $\bar{d}$  is not and the largest drop is achieved around  $A_p \sim 0.06 \pm 0.02$ . The non-monotonous behavior originates from the competition between the heating effects and the pairing<sup>39</sup>. In Fig. 1 e) the time evolution of the  $g(j, t)$  under the influence of the optical pulse is presented as a density plot conjointly with the time evolution of the pulse,  $V(t)$ . We observe a distinct increase of the double occupancy, given by  $g(0, t)$  that peaks around  $t \sim 40$ . The increased double occupancy persists even long after the pulse has been switched off creating a very long-lived (metastable) state, which for the case of Einstein phonons persist almost undistorted up to the largest times used in our calculation. This is consistent also with a time-averaged  $\bar{g}(j)$  as seen in Fig. 1 a) displaying a peak at  $j = 0$  in a sharp contrast with its value in the ground state  $g(j, 0)$ . These observations are in a stark contrast to the Floquet-type scenario analyzed in Ref. 18, where the attractive interaction is induced only during the pulse and in the following we will show that it originates from photo-modified self-trapping.

Now, we will explore how the long-lived state emerges due to the substantial absorption of the total energy predominantly stored in the increased number of phonon excitations. It is thus worthwhile determining the distribution of the number of phonons as a function of the relative distance between the electrons  $j$ . It is measured via the time evolution of  $\gamma(j, t) = \langle \hat{\gamma}(j) \rangle_t$  where

$$\hat{\gamma}(j) = \hat{g}(j) \sum_l a_l^\dagger a_l, \quad (3)$$

describes the total number of phonons in states where the distance between electrons equals  $j$ . As it is shown in Fig. 1 f), most of the excess phonon excitations are absorbed by doubly

occupied states, i.e.  $j = 0$ , and those where electrons are in close proximity. It seems as if the excess phonon excitations represent the *glue* that at least for the given driving frequency  $\omega_d/\omega_0 = 0.9$  provides a self-trapped attractive potential.

Searching further for the origin of the optically induced electron-electron potential we realize that it can only originate from the non-linear electron-phonon interaction term in Eq. (1), i.e. from the term  $H_{g2} = g_2 \sum_j \hat{n}_j (a_j^\dagger + a_j)^2$ . We define an effective potential by projecting  $H_{g2}$  on a subspace with a specified distance between electrons:

$$\hat{v}(j) = \hat{g}(j) H_{g2}, \quad (4)$$

that yields the time evolution of the effective potential  $v(j, t) = \langle \hat{v}(j) \rangle_t$ . This definition is further justified by the sum-rule that gives the total interacting energy  $\sum_j v(j, t) = E_{g2}(t)$  shown in Fig. 1 b).

Motivated by previous Floquet analysis<sup>18</sup> and a driven atomic limit analysis, see SM<sup>47</sup>, predicting attractive (repulsive) electronic interaction for driving below (above) lattice frequency, we present  $v(j, t)$  for two distinct driving frequencies leading to attractive  $\omega_d/\omega_0 = 0.9$  and repulsive  $\omega_d/\omega_0 = 1.1$  interaction for  $g_2 = -0.12$ , see Figs. 2 a) and b). When  $\omega_d/\omega_0 = 0.9$  the pulse generates a pronounced peak located at  $j = 0$ , signaling the attractive effective potential that is most negative for the doubly occupied site. This is also presented in Fig. 2 c) where we show time averaged  $\bar{v}(j)$ . In contrast, at  $\omega_d/\omega_0 = 1.1$ , two minima appear around  $j \pm 10$  that are further apart than the shallow minima in the ground state at  $t = 0$ , most clearly observed in Fig. 2 c). This is consistent with repulsive interaction considering that our computations are performed on a finite-size system. In Fig. 2 d) we further investigate the dependence of the effective potential on  $\omega_d$ . We present time-averaged  $\bar{v}(j)$  computed using different driving frequencies  $\omega_d$ . While the strongest attractive interaction is observed around  $\omega_d/\omega_0 = 0.9$ , with increasing  $\omega_d$  the minimum at  $j = 0$  splits into two separate minima, consistent with the onset of a repulsive interaction. Around  $\omega_d/\omega_0 = 1.1$  the separation of the local minima reaches its largest value  $|j| \sim 10$ . With further increase of  $\omega_d$  the depth of the local minima diminishes and merges with the background. The presence of the minima after the pulse is in a clear distinction with the Floquet analysis, where the response is present only during the pulse. The dynamics of  $v(j)$  shows that this interaction originates from the dynamical modification of the trapping potential leading to a long-lived state.

To obtain a deeper insight into this phenomenon we compute the time-averaged  $\bar{g}(j)$  and the time averaged  $\bar{\gamma}(j)$  and perform a scan over  $\omega_d$  at  $g_2 = -0.12$ , see Figs 3 a) and b), respectively. For  $\omega_d/\omega_0 \lesssim 0.8$  and  $\omega_d/\omega_0 \gtrsim 1.3$ ,  $\bar{g}(j)$  resembles its value in the ground state before the pulse has been switched on. This is consistent with the lack of the absorbed energy from the pulse as seen in Fig. 3 b) where we observe only a tiny amount of excess phonon excitations in the same  $\omega_d$  regime. Near  $\omega_d/\omega_0 \sim 0.9$ ,  $\bar{g}(j)$  shows a pronounced maximum due to an increased weight of doubly occupied states ( $j = 0$ ) consistent with an attractive electron-electron interaction. With increasing  $\omega_d$  the attractive nature of interactions switches towards a repulsive one as the maximum of

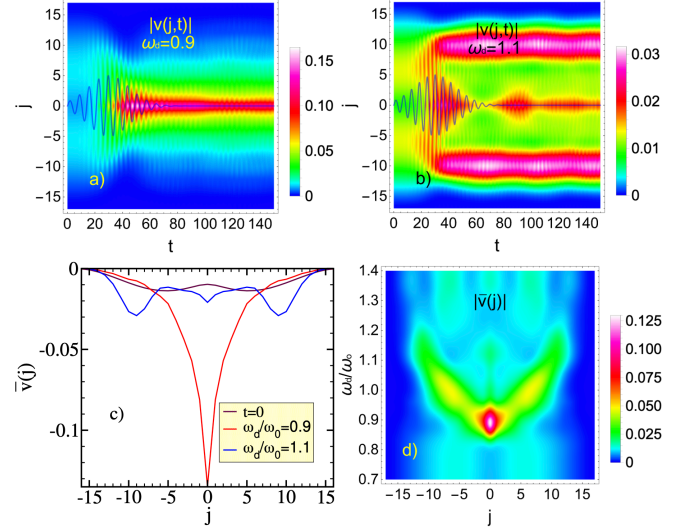


Figure 2: a) and b) magnitude of the effective potential  $|v(j, t)|$  computed with two distinct driving frequencies  $\omega_d/\omega_0 = 0.9$  and  $1.1$ , respectively. Note that the sign of  $v(j, t)$  is strictly negative since  $g_2 = -0.12$ ; c) the effective potential in the ground state,  $v(j, 0)$ , and time-averaged  $\bar{v}(j)$  for two distinct  $\omega_d$ . Time averages were performed in the same interval as in Fig. 1 a); d) time-averaged  $\bar{v}(j)$  for different  $\omega_d$ . We have used the pulse amplitude  $A_p = 0.06$  while the other parameters are identical to those used in Fig. 1.

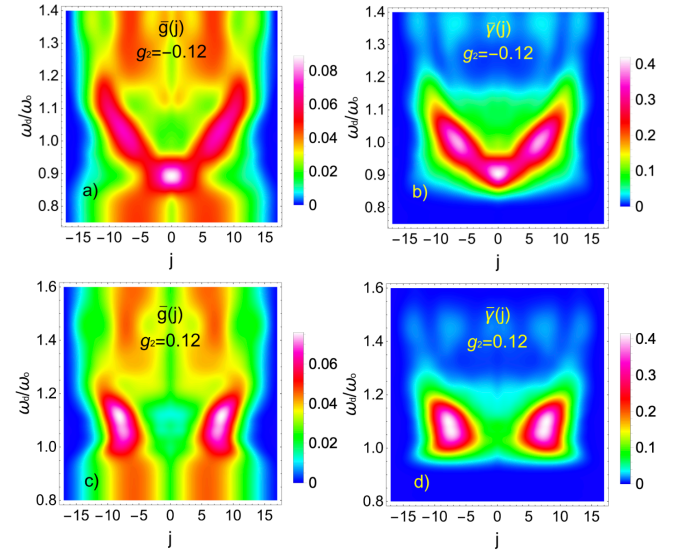


Figure 3: a) and c) the time-averaged density-density correlation function  $\bar{g}(j)$  computed using different driving frequencies  $\omega_d$  for  $g_2 = -0.12$  and  $0.12$ , respectively; b) and d) time-averaged phonon distribution function  $\bar{\gamma}(j)$ . In all cases the time averages were performed in the same interval as in Figs. 1 a) and 2 d). We have used the pulse amplitude  $A_p = 0.06$  while the rest of parameters are identical to those used in Fig. 1.

$\bar{g}(j)$  moves towards larger values of  $j$ . At  $\omega_d/\omega_0 \sim 1.1$  the maximal value of  $\bar{g}(j)$  appears around  $j \sim \pm 10$  that exceeds its average value in the ground state signaling a strengthening

of the repulsive interaction.

The evolution of  $\bar{g}(j)$  caused by changing driving frequencies  $\omega_d$  is closely followed by the evolution of the absorbed phonon excitation distributions,  $\bar{\gamma}(j)$ , shown in Fig. 3 b). It is crucial to stress that time averages are performed in the regime where the optical pulse  $V(t)$  that couples to all oscillators has been switched off. When the pulse is off-resonance, i.e. when  $\omega_d/\omega_0 \gg 1$  or  $\omega_d/\omega_0 \ll 1$ , the system does not absorb much energy consequently,  $\bar{\gamma}(j) \sim 0$  and  $\bar{g}(j)$  remains close to its ground state value. It is worth pointing out that the maximum in the absorbed energy, presented in Fig. 3 b), appears at  $\omega_d/\omega_0 \sim 0.96$  which is just above the value  $\omega_d/\omega_0 \sim 0.9$  where maximal attractive interaction is observed. All this analysis shows that exactly at the resonance the heating effect dominates, but slightly below (above) the binding (repulsion) can win and remarkably leads to a very long-lived state due to the self-trapping mechanism.

In Figs. 3 c) and d) we show results for positive  $g_2 = 0.12$ . Absorption of energy from the pulse appears at higher  $\omega_d$  than in the case when  $g_2 < 0$ , which is consistent with the increase of the phonon frequency in the presence of finite electron density for  $g_2 > 0$ . In contrast to  $g_2 < 0$  case, the absorption of energy always leads to repulsive interaction. The observation contrasts with previous analysis<sup>18,36,38,40</sup> based on the atomic limit or perturbative arguments, which predicted sign-independent pairing. Suppose this observation survives beyond the dilute limit. In that case, it poses a strong constraint on materials where we can expect light-induced long-lived attractive interaction due to the nonlinear electron-lattice couplings.

In the SM<sup>47</sup> we show that two successive optical pulses can switch between attractive and repulsive electron-electron interactions. This result shows that modifying the self-trapping potential can be reversed and we can manipulate it using a proper excitation protocol.

Finally, we explore the long-lived stability of the optically driven attraction between electrons as seen in Fig. 1 e) against the introduction of optical phonon dispersion. In Figs. 4 a) and b) we show  $g(j, t)$  and  $\gamma(j, t)$  obtained from a modified hamiltonian  $H = H_0 - W_{ph}/4 \sum_j (a_j^\dagger a_{j+1} + H.c.)$ . The second term introduces dispersion among optical phonons with the bandwidth  $W_{ph}$ . While the initial decrease of  $\bar{d}$  during the pulse, shown in Fig. 4 c), is comparable to  $W_{ph} = 0$  case, we observe a slow relaxation towards  $\bar{d}_\infty < \bar{d}_0$  with a relaxation time  $\tau_{\bar{d}} \sim 50 \gg 1/W_{ph}$  as the pulse is switched off. In contrast, the double occupancy  $D_t = \langle \hat{n}_\uparrow \hat{n}_\downarrow \rangle_t$ , presented in Fig. 4 d), shows a larger increase at finite  $W_{ph}$  during the pulse, followed by a slow decrease with a relaxation time  $\tau_D \sim \tau_{\bar{d}}$  towards  $D_\infty > D_0$  where  $D_0$  and  $\bar{d}_0$  represent their respective values in the equilibrium. Even though the introduction of finite  $W_{ph}$  results in the initial decrease of  $D(t)$  after the pulse, the value of  $D_\infty$  is consistent with the attractive interaction surviving the introduction of  $W_{ph}$ .

In conclusion, we have performed numerically exact time evolution of a bipolaron problem coupled by a non-linear electron-phonon interaction. If the electron-lattice interaction leads to phonon softening  $g_2 < 0$ , a properly tuned uniform optical pulse that couples to dipole-active lattice vibrations

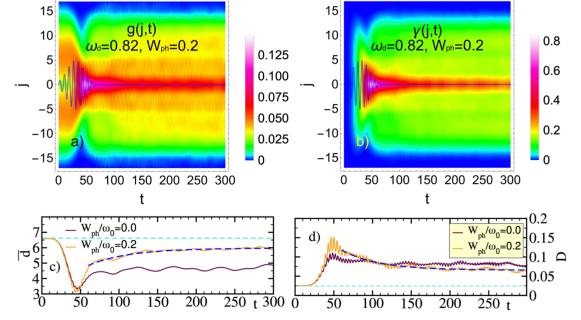


Figure 4: Correlation a)  $g(j, t)$  and b)  $\gamma(j, t)$  for dispersive optical phonons using  $W_{ph} = 0.2$  and optimal driving frequency  $\omega_d/\omega_0 = 0.82$  that at chosen  $W_{ph}$  yields maximal attractive interaction; c) and d) present comparison of  $\bar{d}(t)$  and  $N_{pho}(t)$ , respectively. Exponential fits (blue dashed lines) in c) and d), of the form  $A(t) = \mathcal{A} \exp(-t/\tau) + A_\infty$ , yield  $(\tau_{\bar{d}}, \bar{d}_\infty) \sim (53, 6.0)$  and  $(\tau_D, D_\infty) \sim (48, 0.07)$ , respectively. The other parameters are identical to those used in Figs. 1 e) and f).

may optically induce either attractive or repulsive interaction between electrons. Here the primary mechanism originates from strong dependence of the effective phonon frequency on the local density of electrons<sup>36</sup> so that an appropriately tuned pulse excites phonons corresponding to specific configurations of electrons. The strongest attractive interaction appears when pulses are tuned slightly below the Einstein phonon frequency  $\omega_0$ . This suggests that a softening of the lattice vibration due to an increased electron density and double occupancy plays an essential role in the appearance of the attractive potential between electrons. In contrast, a driving frequency slightly exceeding  $\omega_0$  generates repulsive interaction. In both cases, the effects of optically induced interactions persist long after the pulse has been switched off. Since the energy of the phonon subsystem depends on the density of electrons, both subsystems build an effective trap potential that mutually stabilizes the spatial configurations of electrons and phonons. We have demonstrated that this mechanism is efficient also for weakly dispersive phonons when appropriately tuned laser pulse induces long-living electron-bound states. An important future problem is extending the bipolaron problem to finite doping to understand if we can induce coherence between these highly excited composite particles and to explore the experimental consequences of such states.

### Acknowledgments

J.B., D.G. and K.K. acknowledge the support by the program No. P1-0044 and No. J1-2455 of the Slovenian Research Agency (ARRS). J.B. acknowledge support from the Center for Integrated Nanotechnologies, a U.S. Department of Energy, Office of Basic Energy Sciences user facility. M.M.



acknowledges support by the National Science Centre, Poland

via Project No. 2020/37/B/ST3/00020.

- <sup>1</sup> D. N. Basov, R. D. Averitt, and D. Hsieh, *Nature Materials* **16**, 1077 (2017), URL <https://doi.org/10.1038/nmat5017>.
- <sup>2</sup> C. Giannetti, M. Capone, D. Fausti, M. Fabrizio, F. Parmigiani, and D. Mihailovic, *Advances in Physics* **65**, 58 (2016), <https://doi.org/10.1080/00018732.2016.1194044>, URL <https://doi.org/10.1080/00018732.2016.1194044>.
- <sup>3</sup> P. Salén, M. Basini, S. Bonetti, J. Hebling, M. Krasilnikov, A. Y. Nikitin, G. Shamuilov, Z. Tibai, V. Zhaunerchyk, and V. Goryashko, *Physics Reports* **836-837**, 1 (2019), ISSN 0370-1573, matter manipulation with extreme terahertz light: Progress in the enabling THz technology, URL <https://www.sciencedirect.com/science/article/pii/S0370157319302649>.
- <sup>4</sup> A. de la Torre, D. M. Kennes, M. Claassen, S. Gerber, J. W. McIver, and M. A. Sentef, *Rev. Mod. Phys.* **93**, 041002 (2021), URL <https://link.aps.org/doi/10.1103/RevModPhys.93.041002>.
- <sup>5</sup> A. Kirilyuk, A. V. Kimel, and T. Rasing, *Rev. Mod. Phys.* **82**, 2731 (2010), URL <https://link.aps.org/doi/10.1103/RevModPhys.82.2731>.
- <sup>6</sup> M. Först, R. I. Tobey, S. Wall, H. Bromberger, V. Khanna, A. L. Cavalieri, Y.-D. Chuang, W. S. Lee, R. Moore, W. F. Schlotter, et al., *Phys. Rev. B* **84**, 241104 (2011), URL <https://link.aps.org/doi/10.1103/PhysRevB.84.241104>.
- <sup>7</sup> J. H. Mentink, K. Balzer, and M. Eckstein, *Nature Communications* **6**, 6708 (2015), URL <https://doi.org/10.1038/ncomms7708>.
- <sup>8</sup> T. F. Nova, A. Cartella, A. Cantaluppi, M. Först, D. Bossini, R. V. Mikhaylovskiy, A. V. Kimel, R. Merlin, and A. Cavalleri, *Nature Physics* **13**, 132 (2017), URL <https://doi.org/10.1038/nphys3925>.
- <sup>9</sup> M. Rini, R. Tobey, N. Dean, J. Itatani, Y. Tomioka, Y. Tokura, R. W. Schoenlein, and A. Cavalleri, *Nature* **449**, 72 (2007), URL <https://doi.org/10.1038/nature06119>.
- <sup>10</sup> H. Okamoto, H. Matsuzaki, T. Wakabayashi, Y. Takahashi, and T. Hasegawa, *Phys. Rev. Lett.* **98**, 037401 (2007), URL <https://link.aps.org/doi/10.1103/PhysRevLett.98.037401>.
- <sup>11</sup> S. Kaiser, S. R. Clark, D. Nicoletti, G. Cotugno, R. I. Tobey, N. Dean, S. Lupi, H. Okamoto, T. Hasegawa, D. Jaksch, et al., *Scientific Reports* **4**, 3823 (2014), URL <https://doi.org/10.1038/srep03823>.
- <sup>12</sup> A. Subedi, A. Cavalleri, and A. Georges, *Phys. Rev. B* **89**, 220301 (2014), URL <https://link.aps.org/doi/10.1103/PhysRevB.89.220301>.
- <sup>13</sup> L. Stojchevska, I. Vaskivskiy, T. Mertelj, P. Kusar, D. Svetin, S. Brazovskii, and D. Mihailovic, *Science* **344**, 177 (2014), <https://www.science.org/doi/pdf/10.1126/science.1241591>, URL <https://www.science.org/doi/abs/10.1126/science.1241591>.
- <sup>14</sup> D. Fausti, R. I. Tobey, N. Dean, S. Kaiser, A. Dienst, M. C. Hoffmann, S. Pyon, T. Takayama, H. Takagi, and A. Cavalleri, *Science* **331**, 189 (2011), <https://www.science.org/doi/pdf/10.1126/science.1197294>, URL <https://www.science.org/doi/abs/10.1126/science.1197294>.
- <sup>15</sup> W. Hu, S. Kaiser, D. Nicoletti, C. R. Hunt, I. Gierz, M. C. Hoffmann, M. Le Tacon, T. Loew, B. Keimer, and A. Cavalleri, *Nature Materials* **13**, 705 (2014), URL <https://doi.org/10.1038/nmat3963>.
- <sup>16</sup> M. Mitrano, A. Cantaluppi, D. Nicoletti, S. Kaiser, A. Perucchi, S. Lupi, P. Di Pietro, D. Pontiroli, M. Riccò, S. R. Clark, et al., *Nature* **530**, 461 (2016), URL <https://doi.org/10.1038/nature16522>.
- <sup>17</sup> M. Knap, M. Babadi, G. Refael, I. Martin, and E. Demler, *Phys. Rev. B* **94**, 214504 (2016), URL <https://link.aps.org/doi/10.1103/PhysRevB.94.214504>.
- <sup>18</sup> M. Babadi, M. Knap, I. Martin, G. Refael, and E. Demler, *Phys. Rev. B* **96**, 014512 (2017), URL <https://link.aps.org/doi/10.1103/PhysRevB.96.014512>.
- <sup>19</sup> A. F. Kemper, M. A. Sentef, B. Moritz, T. P. Devereaux, and J. K. Freericks, *Annalen der Physik* **529**, 1600235 (2017), <https://onlinelibrary.wiley.com/doi/pdf/10.1002/andp.201600235>, URL <https://onlinelibrary.wiley.com/doi/abs/10.1002/andp.201600235>.
- <sup>20</sup> G. Mazza and A. Georges, *Phys. Rev. B* **96**, 064515 (2017), URL <https://link.aps.org/doi/10.1103/PhysRevB.96.064515>.
- <sup>21</sup> N. Bittner, T. Tohyama, S. Kaiser, and D. Manske, *Journal of the Physical Society of Japan* **88**, 044704 (2019), <https://doi.org/10.7566/JPSJ.88.044704>, URL <https://doi.org/10.7566/JPSJ.88.044704>.
- <sup>22</sup> A. Grankin, M. Hafezi, and V. M. Galitski, *Phys. Rev. B* **104**, L220503 (2021), URL <https://link.aps.org/doi/10.1103/PhysRevB.104.L220503>.
- <sup>23</sup> M. Buzzi, D. Nicoletti, M. Fechner, N. Tancogne-Dejean, M. A. Sentef, A. Georges, T. Biesner, E. Uykur, M. Dressel, A. Henderson, et al., *Phys. Rev. X* **10**, 031028 (2020), URL <https://link.aps.org/doi/10.1103/PhysRevX.10.031028>.
- <sup>24</sup> A. F. G. Wyatt, V. M. Dmitriev, W. S. Moore, and F. W. Sheard, *Phys. Rev. Lett.* **16**, 1166 (1966), URL <https://link.aps.org/doi/10.1103/PhysRevLett.16.1166>.
- <sup>25</sup> A. H. Dayem and J. J. Wiegand, *Phys. Rev.* **155**, 419 (1967), URL <https://link.aps.org/doi/10.1103/PhysRev.155.419>.
- <sup>26</sup> G. Eliashberg, *Tech. Rep., Inst. of Theoretical Physics, Moscow* (1970).
- <sup>27</sup> M. Först, C. Manzoni, S. Kaiser, Y. Tomioka, Y. Tokura, R. Merlin, and A. Cavalleri, *Nature Physics* **7**, 854 (2011), URL <https://doi.org/10.1038/nphys2055>.
- <sup>28</sup> A. S. Disa, T. F. Nova, and A. Cavalleri, *Nature Physics* **17**, 1087 (2021).
- <sup>29</sup> A. Subedi, *Comptes Rendus. Physique* **22**, 161 (2021).
- <sup>30</sup> R. Mankowsky, A. Subedi, M. Först, S. O. Mariager, M. Chollet, H. Lemke, J. S. Robinson, J. M. Glowia, M. P. Minitti, A. Frano, et al., *Nature* **516**, 71 (2014).
- <sup>31</sup> V. Esposito, M. Fechner, R. Mankowsky, H. Lemke, M. Chollet, J. M. Glowia, M. Nakamura, M. Kawasaki, Y. Tokura, U. Staub, et al., *Phys. Rev. Lett.* **118**, 247601 (2017), URL <https://link.aps.org/doi/10.1103/PhysRevLett.118.247601>.
- <sup>32</sup> A. Subedi, *Physical Review B* **95**, 134113 (2017).
- <sup>33</sup> T. Nova, A. Disa, M. Fechner, and A. Cavalleri, *Science* **364**, 1075 (2019).
- <sup>34</sup> C. P. J. Adolphs and M. Berciu, *Phys. Rev. B* **89**, 035122

- (2014), URL <https://link.aps.org/doi/10.1103/PhysRevB.89.035122>.
- <sup>35</sup> C. P. J. Adolphs and M. Berciu, Phys. Rev. B **90**, 085149 (2014), URL <https://link.aps.org/doi/10.1103/PhysRevB.90.085149>.
- <sup>36</sup> D. M. Kennes, E. Y. Wilner, D. R. Reichman, and A. J. Millis, Nature Physics **13**, 479 (2017), URL <https://doi.org/10.1038/nphys4024>.
- <sup>37</sup> F. Grandi, J. Li, and M. Eckstein, Phys. Rev. B **103**, L041110 (2021), URL <https://link.aps.org/doi/10.1103/PhysRevB.103.L041110>.
- <sup>38</sup> M. A. Sentef, Phys. Rev. B **95**, 205111 (2017), URL <https://link.aps.org/doi/10.1103/PhysRevB.95.205111>.
- <sup>39</sup> Y. Murakami, N. Tsuji, M. Eckstein, and P. Werner, Phys. Rev. B **96**, 045125 (2017), URL <https://link.aps.org/doi/10.1103/PhysRevB.96.045125>.
- <sup>40</sup> J. Sous, B. Kloss, D. M. Kennes, D. R. Reichman, and A. J. Millis, Nature Communications **12**, 5803 (2021), URL <https://doi.org/10.1038/s41467-021-26030-3>.
- <sup>41</sup> J. Bonča, S. A. Trugman, and I. Batistić, Phys. Rev. B **60**, 1633 (1999).
- <sup>42</sup> J. Bonča, T. Kstrašnik, and S. A. Trugman, Phys. Rev. Lett. **84**, 3153 (2000), URL <https://link.aps.org/doi/10.1103/PhysRevLett.84.3153>.
- <sup>43</sup> L.-C. Ku, S. A. Trugman, and J. Bonča, Phys. Rev. B **65**, 174306 (2002), URL <https://link.aps.org/doi/10.1103/PhysRevB.65.174306>.
- <sup>44</sup> D. Golež, J. Bonča, L. Vidmar, and S. A. Trugman, Phys. Rev. Lett. **109**, 236402 (2012), URL <https://link.aps.org/doi/10.1103/PhysRevLett.109.236402>.
- <sup>45</sup> J. Kogoj, M. Mierzejewski, and J. Bonča, Phys. Rev. Lett. **117**, 227002 (2016), URL <https://link.aps.org/doi/10.1103/PhysRevLett.117.227002>.
- <sup>46</sup> J. Bonča and S. A. Trugman, Phys. Rev. B **103**, 054304 (2021), URL <https://link.aps.org/doi/10.1103/PhysRevB.103.054304>.
- <sup>47</sup> *See the supplemental material at [url will be inserted by publisher] for the description of the numerical method, results obtained with the driving frequency  $\omega_d/\omega_0 = 1.1$ , the response of the system for  $g_2 = 0.5$ , the finite hilbert-space analysis, the double pulse time evolution, and analytic solution of the driven single-site problem.*
- <sup>48</sup> P. T. Jun and J. C. Light, J. Chem. Phys. **85**, 5870 (1986).

# Optical manipulation of bipolarons in a system with nonlinear electron-phonon coupling

K. Kovač,<sup>1,2</sup> D. Golež,<sup>1,2</sup> M. Mierzejewski,<sup>3</sup> and J. Bonča<sup>1,2</sup>

<sup>1</sup>J. Stefan Institute, 1000 Ljubljana, Slovenia

<sup>2</sup>Faculty of Mathematics and Physics, University of Ljubljana, 1000 Ljubljana, Slovenia

<sup>3</sup>Department of Theoretical Physics, Faculty of Fundamental Problems of Technology, Wrocław University of Science and Technology, 50-370 Wrocław, Poland

PACS numbers:

## A. Variational method

The method is based on a construction of basis states for the many-body Hilbert space that can be written as  $|j_1, j_2; \dots, n_m, n_{m+1}, \dots\rangle$ , where the spin up and down electrons are on sites  $j_1$  and  $j_2$ , and there are  $n_m$  phonons on site  $m$ . A variational subspace is constructed iteratively beginning with an initial state where both electrons are on the same site with no phonons and applying the sum of operators  $H_{\text{el}} + H_{\text{EP}}$  ( $H_{\text{el}} = \sum_{j,s} (c_{j,s}^\dagger c_{j+1,s} + \text{H.c.})$  and  $H_{\text{EP}} = \sum_j \hat{n}_j (a_j^\dagger + a_j) N_h$  times taking into account the full translational symmetry. The constructed variational Hilbert space defined on the one-dimensional chain allows only a finite maximal distance of a phonon quanta from the doubly occupied site,  $L_{\text{max}_1} = (N_h - 1)/2$ , a maximal distance between two electrons  $L_{\text{max}_2} = N_h$ , and a maximal amount of phonon quanta at the doubly occupied site  $N_{\text{phmax}} = N_h$ . The number of states in the many-body Hilbert space  $N_{\text{st}}$  increases with  $N_h$  exponentially as  $N_{\text{st}} \sim 6.4 \times 2^{1.02N_h}$ .

## B. Driving with $\omega_d/\omega_0 = 1.1$

In Fig. 1 we present the time evolution of  $g(j, t)$  and  $\gamma(j, t)$  under the influence of the optical pulse with the driving frequency  $\omega_d/\omega_0 = 1.1$  that generates repulsive interaction between the electrons. In comparison to the case presented in Fig. 1e) where the central driving frequency is  $\omega_d/\omega_0 = 0.9$ , where maximum of  $g(j, t)$  after the pulse is switched off is around  $j \sim 0$ , in Fig. 1 a) the peak in  $g(j, t)$  is around  $j \sim 10$ . In addition, the increase of  $\gamma(j, t)$  is more evenly spread to  $j \neq 0$  in Fig. 1 b) than in Fig. 1(f).

## C. Response of the system for $g_2 > 0$

In Fig. 2 we analyze the response of the system to different driving frequencies in the case of positive quadratic EP coupling  $g_2 = 0.5$ . This analysis has been stimulated by the results presented in Ref.<sup>1</sup> where authors analyze the atomic limit of the model in Eq. (1). They compute the effective electron-electron interaction  $U^*$  of the model by comparing energies of zero, one and two electrons on the atomic site with

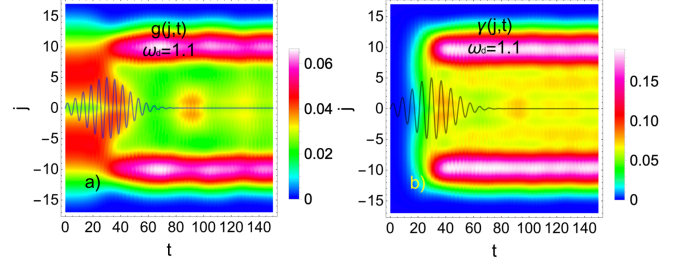


Figure 1: Time-dependent correlation functions at  $\omega_d/\omega_0 = 1.1$ . a) the density-density correlation function  $g(j, t)$ ; b) the number of phonons as a function of the inter-electron distance  $\gamma(j, t)$ . In both cases the shape of the pulse  $A(t)$  with  $\omega_d/\omega_0 = 1.1$  is shown, its vertical scale is in arbitrary units. The rest of parameters is the same as used to generate Fig. 1(e) and (f).

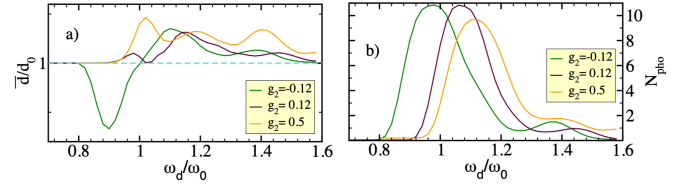


Figure 2: The time-averaged correlation functions computed at  $g_2 = 0.5$  and  $-0.12$  for different driving frequencies  $\omega_d$ . Time averages are defined as in Fig. 3 of the main text; a) represents the time-averaged distance relative to its ground state value  $d_0$ ,  $\bar{d}/d_0$  and b) the total number of phonons  $N_{\text{pho}}$ . The rest of parameters are identical to those used in Fig. (3) of the main text.

an equal number of phonon excitations  $N_{\text{pho}}$  that gives:

$$U^* = U - (N_{\text{pho}} + \frac{1}{2})\omega_0 \left[ 2\sqrt{1 + 4g_2/\omega_0} - 1 - \sqrt{1 + 8g_2/\omega_0} \right]. \quad (1)$$

The second term in Eq. 1 is negative for any finite value of  $g_2 > -\omega_0/8$ , nevertheless, its value is asymmetric around  $g_2 = 0$ . For example, in the case of  $g_2 = -0.12$ , one obtains similar renormalization  $U^*$  as for  $g_2 = 0.5$ . This suggests an inquiry whether a positive  $g_2$  that gives similar renormalization in the atomic limit also leads to attractive interaction when subject to an optical pulse with a well-tuned frequency. In Fig. 2 we show results of time-averaged  $\bar{g}(j)$  and  $\bar{\gamma}(j)$  obtained using identical numerical procedure as used for Fig. (3) of the main text. In contrast to results for  $g_2 = -0.12$ , presented in Fig. (3) a) and c) of the main text, results in Figs. (2) a) and c) show no attractive interaction at any value of  $\omega_d$ .

Instead, for  $\omega_d/\omega_0 \gtrsim 1.0$  results are consistent with repulsive interaction. The only similarity between the two cases is in comparison of Figs. (3) d) of the main text and Fig. 2 d) where  $N_{\text{pho}}$  shows a very similar dependence on  $\omega_d$  apart for a shift to larger  $\omega_d$ . This points to a similar total energy absorption from the pulse but its distribution relative to the electron position  $\bar{\gamma}(j)$  as displayed in Figs. (3) b) of the main text and Fig. 2 b) shows a stark contrast. While for  $g_2 < 0$   $\bar{\gamma}(j)$  peaks at the electron position, at  $j = 0$ , for  $g_2 > 0$   $\bar{\gamma}(j)$  shows a local minimum at  $j = 0$ .

Next, we investigate whether an attractive induced interaction between exists for  $g_2 > 0$ . In Fig. 2(a) and (b) we show time-averaged  $\bar{d}$  and  $N_{\text{pho}}$  as functions of  $\omega_d$  for  $g_2 = -0.12$  and two positive values  $g_2 = 0.12$  and  $0.5$ . For  $g_2 > 0$   $\bar{d}$  always increases, consistent with the repulsive interaction, providing that  $\omega_d$  is chosen such that the system absorbs energy from the pulse that leads to the increase of  $N_{\text{pho}}$ . When comparing results for  $g_2 = -0.12$  and  $+0.12$  we observe a very similar increase of  $N_{\text{pho}}$  with the only observable difference in the shift of  $g_2 = 0.12$  result towards slightly larger  $\omega_d$ . In contrast, for  $g_2 = -0.12$   $\bar{d}$  is consistent with attractive interaction for  $0.8 \lesssim \omega_d/\omega_0 \lesssim 1.0$  and repulsive for  $1.0 \lesssim \omega_d/\omega_0 \lesssim 1.6$ . It is worth stressing that in the latter case, the deep in  $\bar{d}$  is reached around  $\omega_d/\omega_0 = 0.9$  while the peak in  $N_{\text{pho}}$  appears around  $\omega_d/\omega_0 = 0.96$ .

#### D. Finite Hilbert space analysis

In Fig. 3 we show how the time-averaged  $\bar{d}$  changes with increasing size of the Hilbert space  $N_{\text{st}}$  as a function of  $\omega_d$ . Note first that  $N_h$  that sets the number of many-body Hilbert states  $N_{\text{st}} \sim 6.4 \times 2^{1.02N_h}$  also defines the maximal allowed distance between electrons. The decrease of  $\bar{d}$  around  $\omega_d/\omega_0 \sim 0.9$  seems to be well converged in terms of the optimal value of  $\omega_d$  that yields maximal drop of  $\bar{d}$  as well as its relative change  $\bar{d}/d_0$ . In contrast, the increase of  $\bar{d}/d_0$  that indicates repulsion at  $\omega_d/\omega_0 > 1$  grows in size. This is consistent with the repulsive nature of interaction taking into account limited distance between the electrons due to the restricted Hilbert space. In the inset of Fig. 3 we show  $d_0$  in the ground state for different  $N_h$ . Even though the average distance  $d_0$  before the application of the pulse increases with the system size due to finite  $U = 0.5$ , the relative decrease  $\bar{d}/d_0$  seems to converge with increasing  $N_h$  signaling the effectiveness of the optically induced attractive interaction.

#### E. Double pulse

In Fig. 4 we present a simulation of a system with  $g_2 = -0.12$  subject to two consecutive optical pulses with different driving frequencies and amplitudes. The simulation starts from a ground state with  $U = 0.5$  and the average distance between electrons  $\bar{d} \sim 6.5$ . A pulse with  $\omega_{d1}/\omega_0 = 0.9$  is switched on that gives rise to an attractive interaction resulting in a decrease of  $\bar{d}$  as shown in Fig. 4 d) while  $g(j, t)$  peaks around  $j = 0$ , as consistent with the increase of double oc-

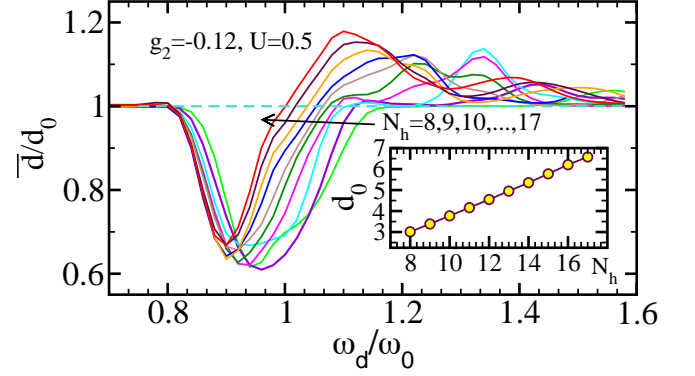


Figure 3: The time-averaged  $\bar{d}/d_0$  for different sizes of the Hilbert space ranging from  $N_{\text{st}} \sim 1600$  for  $N_h = 8$ , up to  $N_{\text{st}} \sim 1.1 \times 10^6$  for  $N_h = 17$ .  $d_0$  represents the average distance in the equilibrium. Note that  $N_h$  represents the maximal distance between electrons and the maximal  $N_{\text{pho}}$ . The inset shows the average distance  $d_0$  in the ground state before the pulse has been switched on. The rest of the parameters are identical to those used in Fig. (3) of the main text.

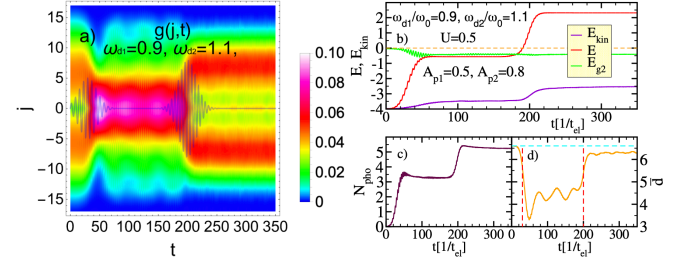


Figure 4: a)  $g(j, t)$  in the case of two successive optical pulses with two different  $\omega_d$  and  $A_p$  as denoted in the legend; b) different energies as defined in the caption of Fig. (1) of the main text; c) and d),  $N_{\text{pho}}$  and  $\bar{d}$ , respectively. In d) vertical lines present times  $t_1 = 45$  and  $t_2 = 200$  of the optical pulses given by  $V(t) = A_{p1} \sin(\omega_{d1}t) \exp[-(t-t_1)^2/2\sigma^2] + A_{p2} \sin(\omega_{d2}t) \exp[-(t-t_2)^2/2\sigma^2]$  as also shown with a grey line in a). The other parameters are identical to those used in Fig. (1) of the main text.

cupancy. The second pulse with  $\omega_{d2}/\omega_0 = 1.1$  results in the increase of  $\bar{d}$  indicating the change of the interaction from attractive to repulsive. Both pulses lead to an increase of the total as well as the kinetic energy,  $E$  and  $E_{\text{kin}}$ , respectively, as seen in Fig. 4 b) and a slight drop of the EP coupling energy  $E_{g2}$ .

#### F. Driven single-site problem (analytic solution)

Numerical simulations show a resonant behavior of the optically driven system. We analyze the driving process analytically in the atomic limit ( $t = 0$ ). The starting point is the



Hamiltonian

$$\mathcal{H}_{at} = U\hat{n}_\uparrow\hat{n}_\downarrow + \omega_0\left(b^\dagger b + \frac{1}{2}\right) + g_2\hat{n}\left(b^\dagger + b\right)^2 + F(t)\left(b^\dagger + b\right). \quad (2)$$

First, we apply the squeezing transformation  $\tilde{\mathcal{H}}_{at} = e^{\hat{S}_1}\mathcal{H}_{at}e^{-\hat{S}_1}$  proposed by Kennes et al.<sup>1</sup> which rescales the position and momentum of oscillators depending on a local electronic density. The generator of squeezing transformation can be written as

$$\hat{S}_1 = \frac{i}{2}\zeta(\hat{x}\hat{p} + \hat{p}\hat{x}) = -\frac{1}{2}\zeta_j\left(b^{\dagger 2} - b^2\right), \quad (3)$$

with the squeezing parameter  $\zeta = -\frac{1}{4}\ln\left(1 + \frac{4g_2\hat{n}}{\omega_0}\right)$ . Bosonic operators are converted into

$$\begin{aligned} b^\dagger &\longrightarrow \tilde{b}^\dagger = b^\dagger \cosh \zeta + b \sinh \zeta \\ b &\longrightarrow \tilde{b} = b \cosh \zeta + b^\dagger \sinh \zeta \end{aligned} \quad (4)$$

while the electron number operator remains unaffected. Hamiltonian takes the following form

$$\tilde{\mathcal{H}}_{at} = U\hat{n}_\uparrow\hat{n}_\downarrow + \omega(\hat{n})\left(b^\dagger b + \frac{1}{2}\right) + F(t)\left(1 + \frac{4g_2\hat{n}}{\omega_0}\right)^{-\frac{1}{4}}\left(b^\dagger + b\right), \quad (5)$$

where  $\omega(\hat{n}) = \omega_0\sqrt{1 + \frac{4g_2\hat{n}}{\omega_0}}$  denotes the electron-density dependent oscillator frequency.

Since  $\tilde{\mathcal{H}}_{at}$  has a similar form as the single-site Holstein-Hubbard Hamiltonian we proceed with a transformation analogous to the Lang-Firsov transformation. Based on the form of the Lang-Firsov transformation generator we construct

$$\hat{S}_2 = \frac{F(t)}{\omega_0}\left(1 + \frac{4g_2\hat{n}}{\omega_0}\right)^{-\frac{3}{4}}\left(b^\dagger - b\right). \quad (6)$$

This transformation maps bosonic operators

$$\begin{aligned} b^\dagger &\longrightarrow b^\dagger - \frac{F(t)}{\omega_0}\left(1 + \frac{4g_2\hat{n}}{\omega_0}\right)^{-\frac{3}{4}} \\ b &\longrightarrow b - \frac{F(t)}{\omega_0}\left(1 + \frac{4g_2\hat{n}}{\omega_0}\right)^{-\frac{3}{4}} \end{aligned} \quad (7)$$

and yields transformed Hamiltonian of the form

$$\mathcal{H}'_{at} = U\hat{n}_\uparrow\hat{n}_\downarrow + \omega(\hat{n})\left(b^\dagger b + \frac{1}{2}\right) - \frac{F(t)^2}{\omega_0}\left(1 + \frac{4g_2\hat{n}}{\omega_0}\right)^{-1}. \quad (8)$$

The electron number operator is once again unaffected by the transformation.

The dependence of the driving response should be reflected in the effective electron-electron interaction which we introduce following Kennes et al.<sup>1</sup> as

$$U_{eff} = (E_2 - E_0) - 2(E_1 - E_0) = E_2 - 2E_1 + E_0, \quad (9)$$

Considering  $\tilde{\mathcal{H}}_{at}$  (we find it more convenient to obtain time-dependencies using  $\tilde{\mathcal{H}}_{at}$  instead of  $\mathcal{H}'_{at}$ ) the effective Coulomb interaction takes the following form

$$\begin{aligned} U_{eff} &= U + \omega(2)\langle b^\dagger b \rangle_2 + \omega_0\langle b^\dagger b \rangle_0 - 2\omega(1)\langle b^\dagger b \rangle_1 \\ &+ \frac{1}{2}\left[\omega(2) + \omega_0 - 2\omega(1)\right] + F(t)\left[\gamma(2)\langle b^\dagger + b \rangle_2 \right. \\ &\left. + \langle b^\dagger + b \rangle_0 - 2\gamma(1)\langle b^\dagger + b \rangle_1\right], \end{aligned} \quad (10)$$

where  $\langle b^\dagger b \rangle_n$  and  $\langle b^\dagger + b \rangle_n$  denote the expectation value of the  $b^\dagger b$  and  $b^\dagger + b$  operators in the propagated state with  $n \in \{0, 1, 2\}$  being the electron occupation number. We introduced  $\gamma(\hat{n}) = \left(1 + \frac{4g_2\hat{n}}{\omega_0}\right)^{-\frac{1}{4}}$  to obtain expression in a more compact form. The electron occupation number operators in  $\omega(\hat{n})$  and  $\gamma(\hat{n})$  can be replaced with scalars in the atomic limit.

We believe that there is a strong correlation between the behavior of  $U_{eff}$  and the expectation number of phonons excited during the driving. Bearing in mind the mapping of bosonic operators (4) the phonon number operator is written as

$$\begin{aligned} \hat{N}_{ph}(t) &= b^\dagger(t)b(t)\left(\cosh^2 \zeta(n) + \sinh^2 \zeta(n)\right) + \sinh^2 \zeta(n) \\ &+ \left(b^\dagger(t)^2 + b(t)^2\right)\sinh \zeta(n)\cosh \zeta(n) \end{aligned} \quad (11)$$

We calculate time evolutions of  $U_{eff}$  and  $\langle \hat{N}_{ph} \rangle_n$  using the Heisenberg picture. For simplicity we assume the harmonic driving  $F(t) = F_0 \sin(\omega_d t)$ . The Heisenberg equations of motion with respect to (5) yield

$$\begin{aligned} b(t) &= be^{-i\omega(n)t} - \frac{iF_0\gamma(n)\omega_d}{\omega(n)^2 - \omega_d^2}\cos(\omega_d t) \\ &\quad - \frac{F_0\gamma(n)\omega_d}{\omega(n)^2 - \omega_d^2}\sin(\omega_d t), \\ b^\dagger(t) &= b^\dagger e^{i\omega(n)t} + \frac{iF_0\gamma(n)\omega_d}{\omega(n)^2 - \omega_d^2}\cos(\omega_d t) \\ &\quad - \frac{F_0\gamma(n)\omega_d}{\omega(n)^2 - \omega_d^2}\sin(\omega_d t), \end{aligned} \quad (12)$$

The initial state of the system is a coherent state  $|\alpha\rangle$  with  $\langle \hat{x}(t=0) \rangle = 0$  and  $\langle \hat{p}(t=0) \rangle = 0$ . Hence  $\Re(\alpha) = 0$  and  $\Im(\alpha) = \frac{F_0\gamma(n)\omega_d}{\omega(n)^2 - \omega_d^2}$ , where  $\alpha$  denotes the eigenvalue of  $b$ .

It follows

$$\begin{aligned}
 \langle b^\dagger(t)b(t) \rangle_n &= \frac{2F_0^2\gamma(n)^2\omega_d^2}{(\omega(n)^2 - \omega_d^2)^2} \left[ 1 - \cos(\omega_d t) \cos(\omega(n)t) \right. \\
 &\quad \left. - \sin(\omega_d t) \sin(\omega(n)t) \right], \\
 \langle b^\dagger(t) + b(t) \rangle_n &= \frac{2F_0\gamma(n)\omega_d}{\omega(n)^2 - \omega_d^2} \left[ \sin(\omega(n)t) - \sin(\omega_d t) \right], \\
 \langle b^\dagger(t)^2 + b(t)^2 \rangle_n &= \frac{2F_0^2\gamma(n)^2\omega_d^2}{(\omega(n)^2 - \omega_d^2)^2} \left[ \sin^2(\omega_d t) - \cos^2(\omega_d t) \right. \\
 &\quad \left. - \cos(2\omega(n)t) + 2\cos(\omega_d t) \cos(\omega(n)t) \right. \\
 &\quad \left. - 2\sin(\omega_d t) \sin(\omega(n)t) \right],
 \end{aligned} \tag{13}$$

which determines the time-evolution of  $\langle \hat{N}_{ph} \rangle_n$  and  $U_{eff}$ .

In Fig. 5 we plot the time-averaged number of phonons along with the time-averaged potential. We have computed  $\langle b^\dagger(t)b(t) \rangle_n$ ,  $\langle b^\dagger(t) + b(t) \rangle_n$  and  $\langle b^\dagger(t)^2 + b(t)^2 \rangle_n$  for each  $n = 0, 1, 2$  as a function of the driving frequency  $\omega_d$ . These values determine the  $\omega_d$ -dependence of  $\langle \hat{N}_{ph} \rangle_n$  and  $U_{eff}$ . We observe a resonant behavior at frequencies that differ from bare molecular oscillator frequency depending on the electron occupation number and the value of the electron-phonon coupling parameter. At frequencies close to  $\omega_0$  and  $\omega(2)$  effective Coulomb interaction increases, however, there is also a strong dip in  $U_{eff}$  centered at  $\omega(1)$ .

The most important contribution to  $U_{eff}$  comes from  $\langle b^\dagger b \rangle_n$ . This term would persist even if the driving stops and has the same resonant behavior as the number of phonons that get excited during the driving process.

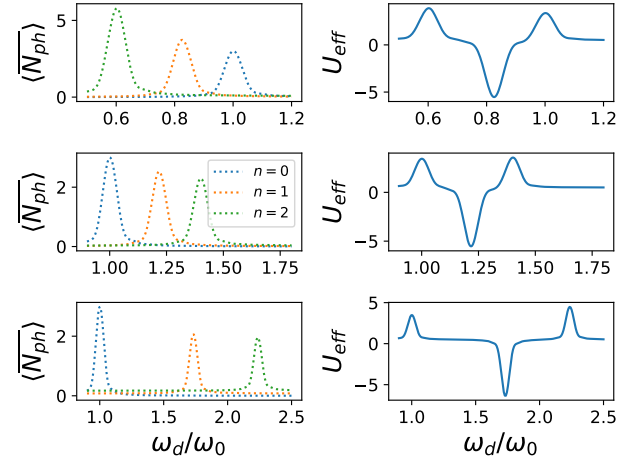


Figure 5: Time-averaged number of phonons and effective potential as a function of the driving frequency. Each row corresponds to a different value of  $g_2$ . The upper one to  $g_2 = -0.08$ , the middle one to  $g_2 = 0.12$  and the bottom one to  $g_2 = 0.5$ .

<sup>1</sup> D. M. Kennes, E. Y. Wilner, D. R. Reichman, and A. J. Millis, Nature Physics **13**, 479 (2017), URL <https://doi.org/10.1038/nphys4024>.